Supplemental Material for

Nonequilibrium molecular dynamics for accelerated computation of ion–ion correlated conductivity beyond Nernst–Einstein limitation

Ryoma Sasaki,[1,2*] Bo Gao,[2] Taro Hirosugi,[1,3] Yoshitaka Tateyama[1,2*]

[1] *School of Materials and Chemical Technology, Tokyo Institute of Technology, Tokyo 152-8552, Japan.*

[2] *Center for Green Research on Energy and Environmental Materials, National Institute for Material Science, Ibaraki 305-0044, Japan.*

[3] *Department of Chemistry, The University of Tokyo, 113-0033, Tokyo. Japan.*

** Corresponding author*

Ryoma Sasaki, School of Materials and Chemical Technology, Tokyo Institute of Technology, Tokyo, 152-8552, Japan. E-mail: sasaki.r.ak@m.titech.ac.jp

Yoshitaka Tateyama, Center for Green Research on Energy and Environmental Materials, National Institute for Material Science, Ibaraki, 305-0044, Japan. E-mail: TATEYAMA.Yoshitaka@nims.go.jp

Supplementary Note 1: Definition of various diffusion coefficients and ionic conductivity

Herein, we clarify the definitions of various diffusion coefficients and the ionic conductivity using the Onsager relationship. For simplicity, we discuss one-dimensional transport. The mass flux along the *x*-direction of species α, J_α, is expressed as:

$$J_\alpha = \frac{1}{V}\sum_{i_\alpha} v_{i_\alpha} = -\sum_{\beta} L^{\alpha\beta}\frac{\partial \bar{\mu}_\beta}{\partial x}, \tag{1}$$

where β is a species, $\bar{\mu}_\beta$ is the electrochemical potential of species β, and $L^{\alpha\beta}$ is the Onsager coefficient related to the Green–Kubo formula and is defined as:

$$L^{\alpha\beta} = \frac{V}{k_\mathrm{B}T}\int_0^\infty \langle J_\alpha(t)\cdot J_\beta(0)\rangle dt, \tag{2}$$

where V and T are the system volume and temperature, respectively, and k_B is the Boltzmann constant. The electrochemical potential of species α is defined as:

$$\bar{\mu}_\alpha = \mu_\alpha^0 + k_\mathrm{B}T\ln a_\alpha + z_\alpha e\phi \tag{3}$$

where μ_α^0, a_α, and z_α are the standard chemical potential, activity, and charge valency of species α, respectively, e is the elementary charge, and ϕ is the electrical potential. Using Eq. (3), Eq. (1) can be rewritten as

$$J_\alpha = -\sum_\beta L^{\alpha\beta} k_\mathrm{B} T \frac{\partial \ln a_\beta}{\partial x} - \sum_\beta L^{\alpha\beta} z_\beta e \frac{\partial \phi}{\partial x} \tag{4}$$

$$= -\sum_\beta L^{\alpha\beta} k_\mathrm{B} T \sum_\gamma \frac{\partial \ln a_\beta}{\partial c_\gamma} \frac{\partial \rho_\gamma}{\partial x} - \sum_\beta L^{\alpha\beta} z_\beta e \frac{\partial \phi}{\partial x} \tag{5}$$

$$= -\sum_\beta L^{\alpha\beta} k_\mathrm{B} T \sum_\gamma \frac{\Theta_{\gamma,\beta}}{\rho_\gamma} \frac{\partial \rho_\gamma}{\partial x} - \sum_\beta L^{\alpha\beta} z_\beta e \frac{\partial \phi}{\partial x} \tag{6}$$

$$= -\frac{L^{\alpha\alpha} k_B T}{\rho_\alpha} \Theta_{\alpha,\alpha} \frac{\partial \rho_\alpha}{\partial x} - \sum_{\beta \neq \alpha} L^{\alpha\beta} k_\mathrm{B} T \sum_\gamma \Theta_{\gamma,\beta} \frac{\partial \rho_\gamma}{\partial x} - \sum_\beta L^{\alpha\beta} z_\beta e \frac{\partial \phi}{\partial x} \tag{7}$$

$$= -\widetilde{D}_\alpha \frac{\partial \rho_\alpha}{\partial x} - \sum_\beta L^{\alpha\beta} z_\beta e \frac{\partial \phi}{\partial x}, \tag{8}$$

$$\text{s.t. } \Theta_{\alpha,\beta} = \rho_\alpha \frac{\partial \ln a_\beta}{\partial \rho_\alpha} = \frac{\partial \ln a_\beta}{\partial \ln \rho_\alpha} = \left(1 + \frac{\partial \ln \gamma_\beta}{\partial \ln \rho_\alpha}\right), \tag{9}$$

where ρ_α, γ_α, $\Theta_{\alpha\beta}$, and $\widetilde{D}_\alpha$ are the number density, activity coefficient, thermodynamics factor, and "chemical diffusion coefficient" of species α, respectively. $\widetilde{D}_\alpha$ is often used for mixed conductors. The $\widetilde{D}_\alpha$ value of a system with two mobile species $\{\alpha, \beta\}$ was derived by using the local charge-neutrality condition [1,2]:

$$\widetilde{D}_\alpha = \frac{z_\alpha^2 L^{\alpha\alpha} z_\beta^2 L^{\beta\beta} - \left(z_\alpha z_\beta L^{\alpha\beta}\right)^2}{z_\alpha^2 L^{\alpha\alpha} + z_\beta^2 L^{\beta\beta} + 2 z_\alpha z_\beta L^{\alpha\beta}} k_B T \left[\frac{1}{z_\alpha^2 \rho_\alpha} \frac{\partial \ln a_\alpha}{\partial \ln \rho_\alpha} + \frac{1}{z_\beta^2 \rho_\beta} \frac{\partial \ln a_\beta}{\partial \ln \rho_\beta}\right] \tag{10}$$

The transport coefficient of $\partial\rho_\alpha/\partial x$ of the first term in Eq. (7)) is called the "transport diffusion coefficient" of species α and is written as $\overline{D}_\alpha$.[3] The transport diffusion coefficient is related to the "self-diffusion (tracer diffusion) coefficient", $D_{\mathrm{self},\alpha}$, as:

$$D_{\mathrm{self},\alpha} = \frac{1}{N_\alpha} \sum_{i_\alpha} \int_0^\infty \langle v_{i_\alpha}(t) v_{i_\alpha}(0) \rangle \mathrm{d}t \tag{11}$$

$$\overline{D}_\alpha = \frac{L^{\alpha\alpha} k_B T}{\rho_\alpha} \Theta_\alpha = \frac{\Theta_\alpha}{N_\alpha} \sum_{i_\alpha} \sum_{j_\alpha} \int_0^\infty \langle v_{i_\alpha}(t) v_{j_\alpha}(0) \rangle \mathrm{d}t \tag{12}$$

$$= \frac{\Theta_\alpha}{N_\alpha} \sum_{i_\alpha} \int_0^\infty \langle v_{i_\alpha}(t) v_{i_\alpha}(0) \rangle \mathrm{d}t + \frac{\Theta_\alpha}{N_\alpha} \sum_{i_\alpha} \sum_{j_\alpha \neq i_\alpha} \int_0^\infty \langle v_{i_\alpha}(t) v_{j_\alpha}(0) \rangle \mathrm{d}t \tag{13}$$

$$= \Theta_\alpha \left[D_{\mathrm{self},\alpha} + \frac{1}{N_\alpha} \sum_{i_\alpha} \sum_{j_\alpha \neq i_\alpha} \int_0^\infty \langle v_{i_\alpha}(t) v_{j_\alpha}(0) \rangle \mathrm{d}t \right] \tag{14}$$

$$= \Theta_\alpha D_{c,\alpha} \tag{15}$$

$$s.t. \quad D_{c,\alpha} = D_{\mathrm{self},\alpha} + \frac{1}{N_\alpha} \sum_{i_\alpha} \sum_{j_\alpha \neq i_\alpha} \int_0^\infty \langle v_{i_\alpha}(t) v_{j_\alpha}(0) \rangle \mathrm{d}t \tag{16}$$

where N_α is the number of particles of species α. $D_{c,\alpha}$ is called the "corrected diffusion coefficient".[3] The coefficient against the gradient of the electric potential, which is the third term in Eq. (8)), is related to the ionic conductivity σ using the Green–Kubo relationship as follows:

$$\sigma = \sum_{\alpha}\sum_{\beta} z_\alpha z_\beta e^2 L^{\alpha\beta} := \sum_{\alpha}\sum_{\beta} \sigma_{\alpha\beta} \tag{17}$$

$$= \frac{e^2}{Vk_BT}\sum_{\alpha}\sum_{\beta}\sum_{i_\alpha}\sum_{i_\beta} z_\alpha z_\beta \int_0^\infty \langle v_{i_\alpha}(t) v_{i_\beta}(0)\rangle \, \mathrm{d}t \tag{18}$$

$$:= \sigma_+^{\text{self}} + \sigma_-^{\text{self}} + \sigma_{++}^{\text{distinct}} + \sigma_{--}^{\text{distinct}} + 2\sigma_{+-}^{\text{distinct}} \tag{19}$$

In Eq. (19), we decompose the conductivity into the self-correlation and distinct terms:

$$\sigma_+^{\text{self}} := \frac{e^2}{Vk_BT}\sum_{\alpha\in\text{cation}} z_\alpha^2 \sum_{i_\alpha}\int_0^\infty \langle v_{i_\alpha}(t) v_{i_\alpha}(0)\rangle \mathrm{d}t = \frac{e^2}{Vk_BT}\sum_{\alpha\in\text{cation}} z_\alpha^2 N_\alpha D_{\text{self},\alpha} \tag{20}$$

$$\sigma_-^{\text{self}} := \frac{e^2}{Vk_BT}\sum_{\alpha\in\text{anion}} z_\alpha^2 \sum_{i_\alpha}\int_0^\infty \langle v_{i_\alpha}(t) v_{i_\alpha}(0)\rangle \mathrm{d}t = \frac{e^2}{Vk_BT}\sum_{\alpha\in\text{anion}} z_\alpha^2 N_\alpha D_{\text{self},\alpha} \tag{21}$$

$$\sigma_{++}^{\text{distinct}} := \frac{e^2}{Vk_BT}\sum_{\alpha\in\text{cation}}\sum_{\beta\in\text{cation}}\sum_{i_\alpha}\sum_{i_\beta\neq i_\alpha} z_\alpha z_\beta \int_0^\infty \langle v_{i_\alpha}(t) v_{i_\beta}(0)\rangle \, \mathrm{d}t \tag{22}$$

$$\sigma_{--}^{\text{distinct}} := \frac{e^2}{Vk_BT}\sum_{\alpha\in\text{anion}}\sum_{\beta\in\text{anion}}\sum_{i_\alpha}\sum_{i_\beta\neq i_\alpha} z_\alpha z_\beta \int_0^\infty \langle v_{i_\alpha}(t) v_{i_\beta}(0)\rangle \, \mathrm{d}t \tag{23}$$

$$\sigma_{+-}^{\text{distinct}} := \frac{e^2}{Vk_BT}\sum_{\alpha\in\text{cation}}\sum_{\beta\in\text{anion}}\sum_{i_\alpha}\sum_{i_\beta} z_\alpha z_\beta \int_0^\infty \langle v_{i_\alpha}(t) v_{i_\beta}(0)\rangle \, \mathrm{d}t \tag{24}$$

The "conductivity diffusion coefficient", "charge diffusion coefficient", or "component diffusion coefficient" $D_{\sigma,\alpha}$ is often used as a quantity with the same dimensions as the diffusion coefficients converted from the conductivity. $D_{\sigma,\alpha}$ is defined based on the electrophoretic mobility u_α. u_α is expressed as [4]:

$$u_\alpha = \sum_\beta L^{\alpha\beta}\frac{z_\beta e}{\rho_\alpha} \tag{25}$$

According to the Einstein–Smoluchowski equation, the conductivity diffusion coefficient, $D_{\sigma,\alpha}$, is related to the mobility via:

$$D_{\sigma,\alpha} = \frac{u_\alpha k_B T}{z_\alpha e} \tag{26}$$

$$= \frac{1}{{z_\alpha}^2 N_\alpha}\sum_\beta z_\alpha z_\beta \sum_{i_\alpha}\sum_{j_\beta}\int_0^\infty \langle v_{i_\alpha}(t) v_{j_\beta}(0)\rangle \, \mathrm{d}t \tag{27}$$

$$= D_{\mathrm{self},\alpha} + \frac{1}{N_\alpha}\sum_{i_\alpha}\sum_{j_\alpha \neq i_\alpha}\int_0^\infty \langle v_{i_\alpha}(t)v_{j_\alpha}(0)\rangle \mathrm{d}t + \frac{1}{{z_\alpha}^2 N_\alpha}\sum_{\beta\neq\alpha} z_\alpha z_\beta \sum_{i_\alpha}\sum_{j_\beta}\int_0^\infty \langle v_{i_\alpha}(t)v_{j_\beta}(0)\rangle \, \mathrm{d}t \quad (28)$$

At the limit of an infinite dilution, all cross-correlation terms such as $\langle v_{i_\alpha}(t)v_{j_{\alpha\neq i_\alpha}}(0)\rangle$ and $\langle v_{i_\alpha}(t)v_{i_\beta}(0)\rangle$ are zero and all activity coefficients are 1, which leads to an equivalence between $\widetilde{D}_\alpha$, $\overline{D}_\alpha$, $D_{\sigma,\alpha}$, and $D_{\mathrm{self},\alpha}$ via Eqs. (14) and (28):

$$\widetilde{D}_\alpha = \overline{D}_\alpha = D_{\sigma,\alpha} = D_{\mathrm{self},\alpha} \quad (29)$$

The conductivity of the dilute system σ_{dilute} is the sum of the self-correlation term of each species, which corresponds to the Nernst–Einstein approximation formula:

$$\sigma_{\mathrm{dilute}} = \frac{e^2}{Vk_BT}\sum_\alpha z_\alpha^2 N_\alpha D_{\mathrm{self},\alpha} \quad (30)$$

Supplementary Note 2. Details of equations of motion

Equilibrium molecular dynamics (EMD) uses the following equations of motion in the *NVT* ensemble:

$$\dot{\mathbf{q}}_i = \frac{\mathbf{p}_i}{m_i} \quad (31)$$

$$\dot{\mathbf{p}}_i = \mathbf{F}_i - \alpha\mathbf{p}_i \quad (32)$$

$$\dot{\alpha} = \frac{1}{Q_1}\left(\sum_i \frac{{\mathbf{p}_i}^2}{m_i} - 3(N-1)k_\mathrm{B}T\right) - \alpha\alpha_2 \quad (33)$$

$$\dot{\alpha_2} = \frac{Q\alpha^2 - k_\mathrm{B}T}{Q_2} - \alpha_2\alpha_3 \quad (34)$$

$$\dot{\alpha_3} = \frac{Q_2\alpha^2 - k_\mathrm{B}T}{Q_3} \quad (35)$$

where q_i, p_i, and F_i are the position, momentum, and force via DFT and color charge of the atom i, respectively. α, Q, and T are the coupling parameter to the Nosé–Hoover chain thermostat (chain length = 3), friction coefficient, and target temperature, respectively.

CCD-NEMD with external field along z-axis use the below equations of motion in the *NVT* ensemble:

$$\dot{\mathbf{q}}_i = \frac{\mathbf{p}_i}{m_i} \quad (36)$$

$$\dot{\mathbf{p}}_i = \begin{cases} F_{i,\{x\ or\ y\}} - \alpha p_{i,\{x\ or\ y\}} \\ F_{i,z} + c_i F_\mathrm{e} \end{cases} \tag{37}$$

$$\dot{\alpha} = \frac{1}{Q_1}\left(\sum_i \frac{p_{i,x}^2 + p_{i,y}^2}{m_i} - 2(N-1)k_\mathrm{B}T\right) \tag{38}$$

where c_i is the color charge of atom i and F_e is the external field. The chain length of the Nosé–Hoover thermostat was equal to 1 for non-equilibrium simulations. If the thermostat is also applied along the z-axis, the effective external force will become $F_\mathrm{e} - \alpha pi$. To avoid deviation of the external force from the setting value F_e, we applied the thermostat on only the x-and y-axes. We used the velocity-Verlet integrator for the time evolution of the equation of motions. The concrete algorithm along the external field (z-axis) with timestep Δt can be written as:

$$p_{i,z}\left(t + \frac{\Delta t}{2}\right) \leftarrow p_i(t) + \left(F_{i,z}(t) + c_i F_\mathrm{e}\right)\frac{\Delta t}{2} \tag{39}$$

$$r_{i,z}(t + \Delta t) \leftarrow r_i(t) + \frac{p_i\left(t + \frac{\Delta t}{2}\right)}{m_i}\Delta t \tag{40}$$

$$p_{i,z}(t + \Delta t) \leftarrow p_i\left(t + \frac{\Delta t}{2}\right) + \left(F_{i,z}(t + \Delta t) + c_i F_\mathrm{e}\right)\frac{\Delta t}{2} \tag{41}$$

The temperature as a function of time, controlled by a thermostat at 1200 K, is shown in Supplementary Figure 1. The temperature was controlled well.

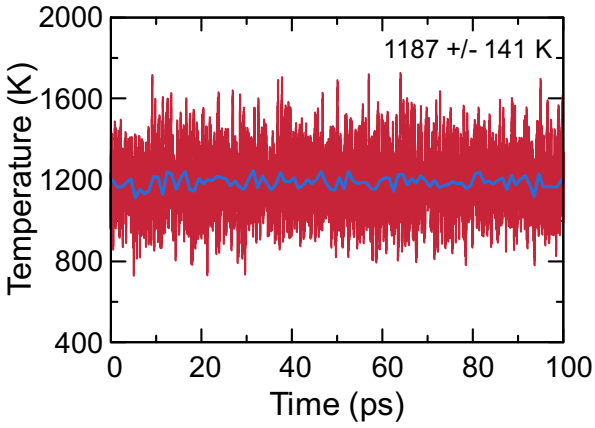

Supplementary Figure 1. Temperature as a function of time for a typical simulation of CCD-NEMD at 1200 K. The blue line represents the 1 ps block averaged value.

Supplementary Note 3. Determination of diffusion coefficients in EMD

The self-diffusion coefficient D_self, charge diffusion coefficient D_σ of Li ions, and conductivity were obtained using the Einstein relation:

$$D_{\mathrm{self}} = \lim_{t\to\infty} \frac{1}{2dtN_{\mathrm{Li}}} \sum_{i\in\mathrm{Li}} \langle [\mathbf{x}_i(t) - \mathbf{x}_i(0)]^2 \rangle \tag{42}$$

$$\mathrm{MSD}_{\mathrm{self}} = \frac{1}{N_{\mathrm{Li}}} \sum_{i\in\mathrm{Li}} \langle [\mathbf{x}_i(t) - \mathbf{x}_i(0)]^2 \rangle \tag{43}$$

$$D_{\sigma} = \lim_{t\to\infty} \frac{1}{2dtN_{\mathrm{Li}}} \sum_{i\in\mathrm{Li},j\in\mathrm{Li,Ge,P,S}} z_i z_j \langle [\mathbf{x}_i(t) - \mathbf{x}_i(0)] \cdot [\mathbf{x}_j(t) - \mathbf{x}_j(0)] \rangle \tag{44}$$

$$\mathrm{MSD}_{\sigma} = \frac{1}{N_{\mathrm{Li}} z_{\mathrm{Li}}^2} \sum_{i\in\mathrm{Li},j\in\mathrm{Li,Ge,P,S}} z_i z_j \langle [\mathbf{x}_i(t) - \mathbf{x}_i(0)] \cdot [\mathbf{x}_j(t) - \mathbf{x}_j(0)] \rangle \tag{45}$$

$$\sigma = \lim_{t\to\infty} \frac{e^2}{2dtVk_{\mathrm{B}}T} \sum_{i,j} z_i z_j \langle [\mathbf{x}_i(t) - \mathbf{x}_i(0)] \cdot [\mathbf{x}_j(t) - \mathbf{x}_j(0)] \rangle \tag{46}$$

where d is the dimension of $\boldsymbol{x}_i(t)$, t is time, N_{Li} is the total number of Li-ions in the simulation cell, $\boldsymbol{x}_i$(t) is the position vector, and z_i is the charge. Supplementary Figure 2 shows the five-sample averaged tracer and collective MSDs at 1200 K. The initial point of the diffusive regime was determined as the time t_{diff}, when the MSD reached 9.0 Å^2, which is large compared to the distance between two neighboring Li site, which is about 2.8 Å, i.e., (2.8 A)^2. In addition, log(t')-log(MSD) was also checked to determine whether t_{diff} is involved in the diffusive regime. The upper fitting bound was determined by t_{diff} × 1.5–4 because the MSD at a larger t had a larger variance and deviation)[5]. The statistical averages were computed from trajectories (140–560 ps; EMD, 100–160 ps; NEMD) tabulated in Supplementary Table 1.

We also investigated the size effect of the DFTMD of LGPS on the conductivity. The results are summarized in the Supplementary Table 2. Although the *ab*-plane conductivity in the smallest model is underestimated by about 30%, there are no severe difference to change the characteristics of the conduction significantly.

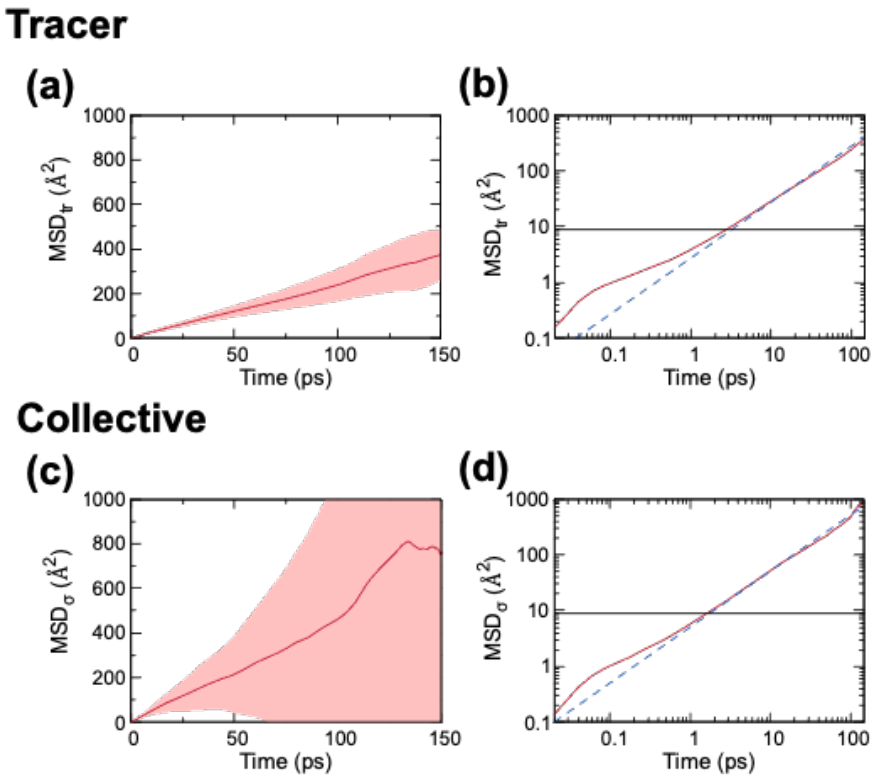

Supplementary Figure 2. (a) (b) Tracer and (c) (d) collective MSD of Li-ions as a function of time. The error bars are standard deviations of the five independent samples.

Supplementary Table 1. Summary of the simulation times of the EMD and the NEMD.

	EMD		NEMD, z direction		NEMD, x direction	
Temperature	Simulation time (ps)	Number of samples	Simulation time (ps)	Number of samples	Simulation time (ps)	Number of samples
1400	160	5	90	5	100	3
1200	160	5	100	5	75	3
1100	160	5	75	5	100	3
1000	240	5	115	5	80	3
900	240	5	80	5	95	3
800	240	5	90	6	100	3
700	400 - 560	10	100	8	240	3
500	400	10	150	10		

Supplementary Table 2. The size effect of the DFTMD of LGPS on the conductivity.

			c-axis			*a*-axis (*ab*-plane)			Number of	
Lx (Å)	Ly (Å)	Lz (Å)	σ_{EMD} (S cm^{-1})	σ_{NEMD} (S cm^{-1})	σ_{dilute} (S cm^{-1})	σ_{EMD} (S cm^{-1})	σ_{NEMD} (S cm^{-1})	σ_{dilute} (S cm^{-1})	Li-ions	atoms
8.719	8.719	12.6	7.5 ± 2.5	7.6 ± 0.9	2.3 ± 0.4	1.7 ± 0.9 (1.7 ± 0.8)	1.3 ± 0.1	0.90 ± 0.09 (0.93 ± 0.13)	20	50
17.44	17.44	12.6	6.3 ± 1.8	6.7 ± 0.7	2.9 ± 0.2	2.5 ± 0.9 (2.2 ± 0.7)	2.4 ± 0.2	1.3 ± 0.1 (1.3 ± 0.1)	80	200
17.44	17.44	25.3	8.7 ± 1.5	7.7 ± 0.3	2.52 ± 0.09	1.7 ± 0.5 (2.3 ± 1.3)	2.2 ± 0.2	1.30 ± 0.04 (1.31 ± 0.04)	160	400

Supplementary Note 4. Field-dependent Flux

Supplementary Figure 3 shows the Li-ion flux along the *c*-axis at 500 K and the *a*-axis at 700 K in the $Li_{10}GeP_2S_{12}$ system as a function of the external field strength F_e. Both linear regimes were identified between 0–0.02 eV. The maximum field strength F_{em}, which is sufficiently small to exhibit a linear response, is expressed as $F_{em} \propto \sqrt{D}^6$. Therefore, F_e = 0.02 eV Å^{-1} is small enough to calculate the conductivity along the *c*- and *a*-axes more than 500 K and 700 K, respectively. Note that 0.02 eV Å^{-1} has been the typical value of some NEMD studies on Li-ion conductors[7–9].

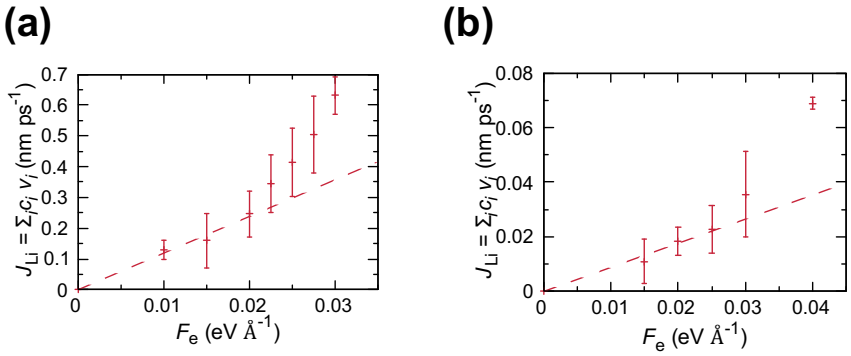

Supplementary Figure 3. Li-ion flux along *c*-axis at (a) 500 K and *a*-axis at (b) 700 K as a function of the external field strength.

Supplementary Note 5. Comparison between CCD-NEMD and CD-NEMD

Supplementary Figure 4 shows the color displacements of CCD-NEMD and CD-NEMD at 500 K with F_e = 0.02 eV Å^{-1} along the *c*-axis. The slope of the color displacements is equal to the color fluxes:

$$\frac{\mathrm{d}}{\mathrm{d}t}\left[\sum_i c_i[z_i(t) - z_i(0)]\right] = \sum_i c_i v_{i,z}(t) = J_c(t) \tag{47}$$

The slope of the color displacements of the CD-NEMD is smaller than that of CCD-NEMD because CD-NEMD does not include the ion–ion correlation term. The conductivity of CD-NEMD is consistent with the Nernst–Einstein approximation result for EMD (Supplementary Table 2) within a standard deviation.

Supplementary Figure 5 shows that the relationship between the color displacements and the averaged color charges in each conduction channel. The color flux occurs even if all the color charges in every channel do not have the same sign.

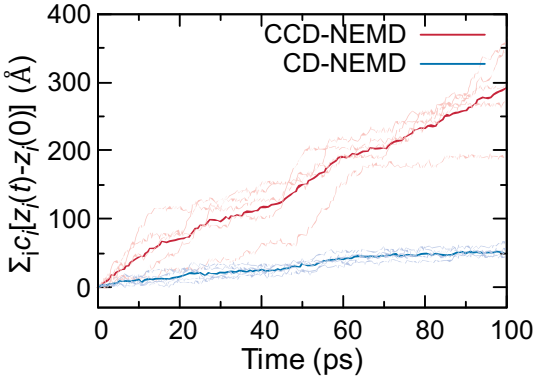

Supplementary Figure 4. Color displacements of CCD-NEMD and CD-NEMD at 500 K with F_e = 0.02 eV Å^{-1} along the *c*-axis. The dark lines show the averaged values of the five independent samples, which are indicated by the lighter lines.

Supplementary Table 2. Comparison of the conductivities at 500 K between σ_{EMD} (EMD with Eq. (46)), $\sigma_{CCD\text{-}NEMD}$ (CCD-NEMD with Eq.(8)), $\sigma_{CD\text{-}NEMD}$ (CD-NEMD with Eq. (5) and Nernst–Einstein approximation of Eq. (30), and σ_{dilute} (EMD with Nernst–Einstein approximation).

σ_{EMD} (S cm^{-1})	$\sigma_{CCD\text{-}NEMD}$ (S cm^{-1})	$\sigma_{CD\text{-}NEMD}$ (S cm^{-1})	σ_{dilute} (S cm^{-1})
1.3 ± 0.6	2.3 ± 0.7	0.35 ± 0.18	0.53 ± 0.18

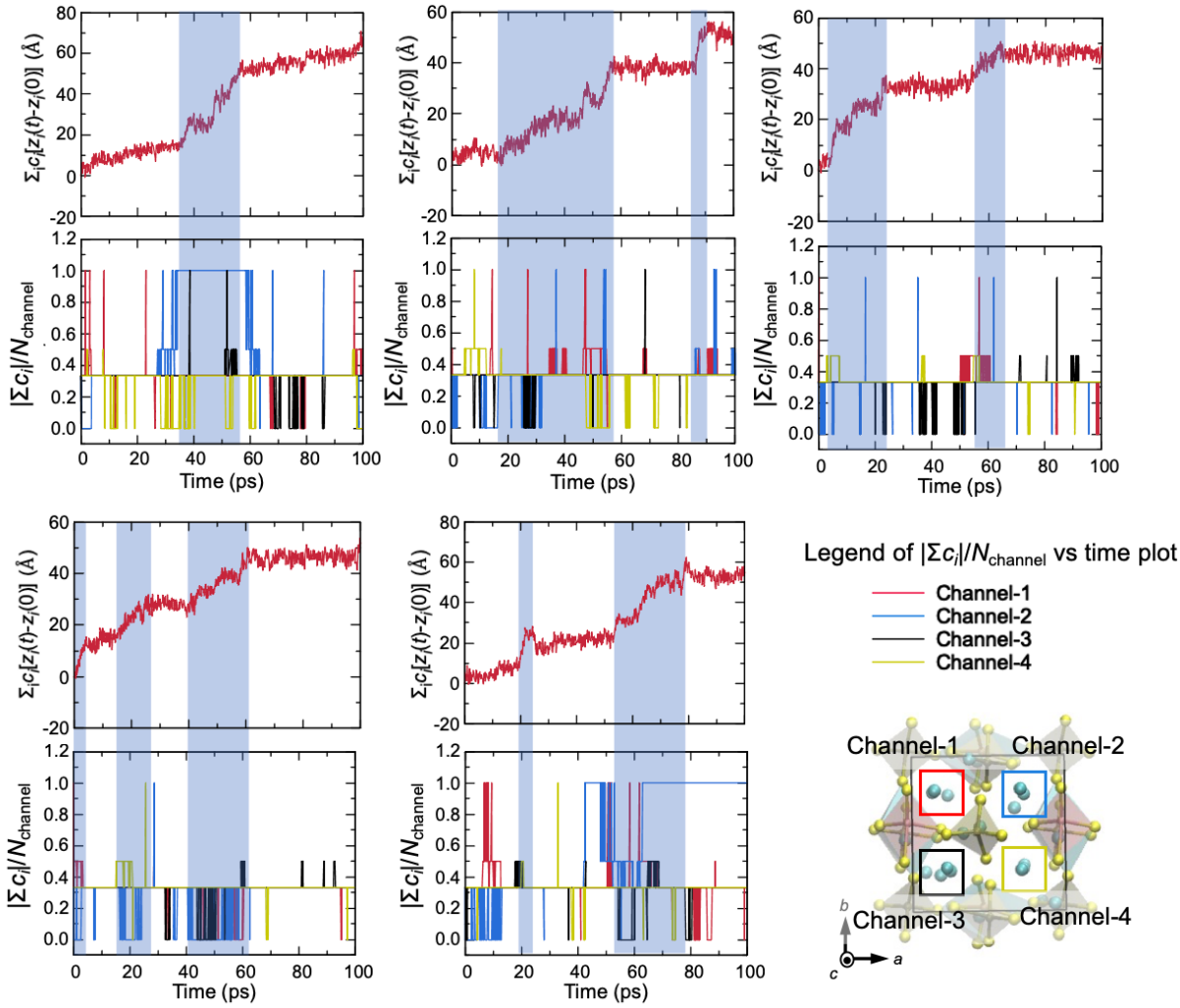

Supplementary Figure 5 Color displacements and absolute values of the averaged color charges within each conduction channel (Channel 1–4) obtained by five independent CD-NEMD calculations (F_e = 0.02 eV Å^{-1} along the *c*-axis) at 500 K. The shaded area denotes the region with a large slope related to the color displacements.

Supplementary Note 6. CCD-NEMD on an oxide-type Li-ion solid electrolyte ($Li_7La_3Zr_2O_{12}$)

We also performed CCD-NEMD simulations using a representative oxide-type Li-ion solid electrolyte, namely $Li_7La_3Zr_2O_{12}$ (LLZO), as shown in Supplementary Figure 6. The strength of the color field was 0.02 eV Å^{-1}, which was within the linear response region, as shown in Supplementary Figure 7. Supplementary Figure 8 shows the cumulative averages of σ_{dilute}, σ_{EMD}, and σ_{NEMD} at 1200 K as a function of time along the *z*-direction. The lines and error bars in Supplementary Figure 8(a) denote the average values and standard deviations of the five independent samples with different initial velocities, respectively. σ_{NEMD} and σ_{EMD} are in good agreement, which demonstrates that CCD-NEMD can

appropriately reflect the contributions of the ion–ion correlation. As shown in Supplementary Figure 8(a) and S8(b), CCD-NEMD can calculate conductivities faster than EMD.

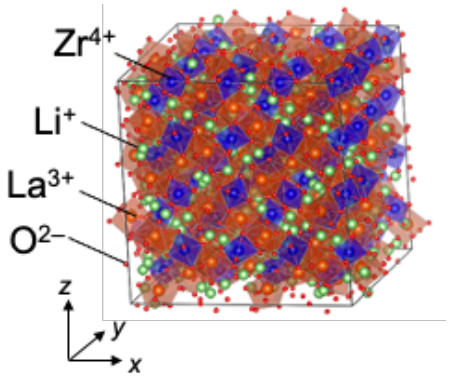

Supplementary Figure 6. Equilibrated structure of 64 $Li_7La_3Zr_2O_{12}$ (26.264×26.264×26.264 $Å^3$) at 1000 K.

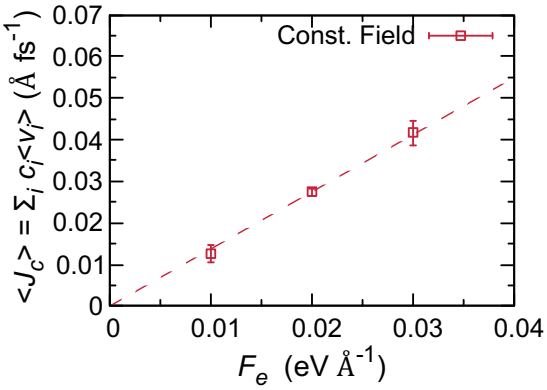

Supplementary Figure 7. Ion flux along the *z*-axis at 1000 K as a function of the external field strength.

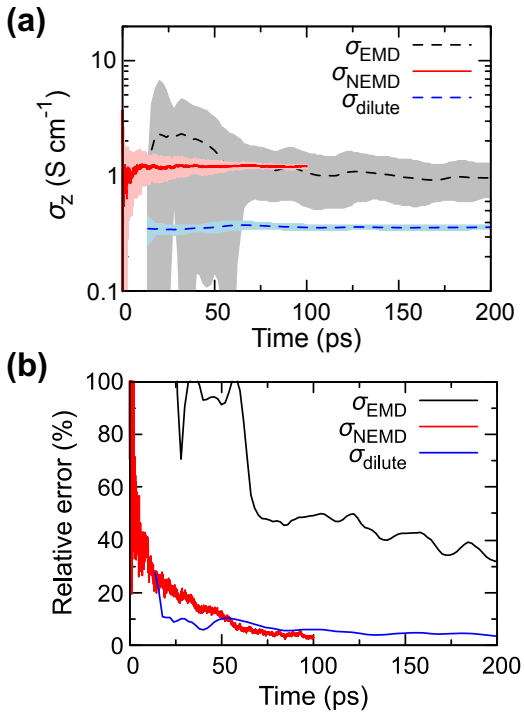

Supplementary Figure 8. Cumulative averaged conductivities (σ_{dilute}, σ_{EMD}, and σ_{NEMD}) and relative errors along the z-axis at 1000 K.

Supplementary Note 7. Interfacial self-diffusion coefficient of the Lennard–Jones binary component system

We evaluated the position-dependent transport property in CD-NEMD. To validate this method, we constructed phase-separated binary Lennard–Jones (LJ) liquid systems, as shown in Supplementary Figure 9(a), and applied CD-NEMD ($c_i = (-1)^i$). The local flux and local self-diffusion coefficient parallel to the interface on each slab k were obtained using the equations:

$$J_{\mathrm{slab}-k}(t) = \sum_{i \in \mathrm{slab}-k} c_i v_i(t) \tag{48}$$

$$D_{\mathrm{slab}-k} \approx \frac{k_\mathrm{B}T}{\langle N_{\mathrm{slab}-k} \rangle} \lim_{t\to\infty} \frac{\langle J_{\mathrm{slab}-k}(t) \rangle}{F_e} \tag{49}$$

The position-dependent self-diffusion coefficients are presented in Supplementary Figure 9(b). The diffusivity increases close to the interfacial region. As the attractive interaction parameter ε_{12} between heterogeneous particles becomes smaller, the enhancement becomes larger. This interfacial enhancement originates from the weaker attractive interaction between heterogeneous particles than between identical particles in the model.[10] It should be noted that the above formulation of CD-NEMD is applicable to CCD-NEMD, where the self-diffusion coefficient of Eq. (49) is replaced with D_σ in the

CCD-NEMD simulation of composite solid electrolytes. This indicates that CCD-NEMD could also be used to estimate the interfacial conductivity.

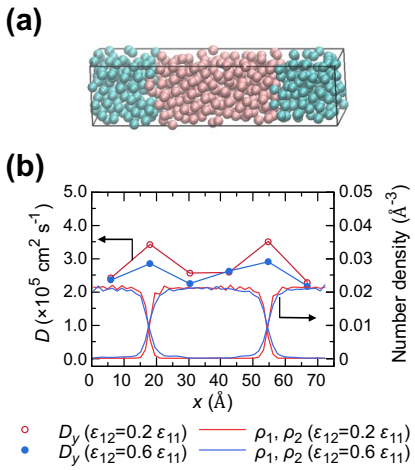

Supplementary Figure 9. (a) Snapshot of an equilibrated structure and (b) position-dependent diffusivity of a Lennard–Jones binary component system.

Model of the interfacial Lennard–Jones binary component system.

The interaction between the LJ particles is the LJ 12-6 potential φ(r) with a cutoff radius of 7.65 Å:

$$\phi(r) = 4\epsilon_{ij}\left[\left(\frac{\sigma_{ij}}{r}\right)^{12} - \left(\frac{\sigma_{ij}}{r}\right)^{6}\right] \tag{50}$$

where r is the distance between the atoms i and j. The parameters ε and σ between the same type of particles are $\varepsilon_{11} = \varepsilon_{22} = 0.238$ kcal mol^{-1} and $\sigma_{11} = \sigma_{22} = 3.4$ Å, which relate to the argon atom.[11] To construct the liquid-liquid interfacial system, the interaction between the different types of atoms was scaled as $\varepsilon_{12} = 0.2\ \varepsilon_{11}$ and $0.6\ \varepsilon_{11}$. The interfacial binary-component system consisted of $N_1 = N_2 = 250$ particles in a simulation box of 18.2 × 18.2 × 72.8 Å^3. The temperature was kept at 94.4 K. The system was equilibrated for 100 ps, and a production run was performed for 400 ps with $F_e = 0.002$ eV Å^{-1}.

Supplementary references

1. Weppner, W. & Huggins, R. A. Determination of the Kinetic Parameters of Mixed-Conducting Electrodes and Application to the System Li3Sb. *J. Electrochem. Soc.* **124**, 1569–1578 (1977).
2. Frenning, G. *Charged Particle Transport: As Information Source about Ion Conductors, Dielectric Materials, and Drug Delivery Systems*. (PhD thesis, University of Uppsala, 2002).
3. Dubbeldam, D. & Snurr, R. Q. Recent developments in the molecular modeling of diffusion in nanoporous materials. *Mol. Simul.* **33**, 305–325 (2009).
4. Fong, K. D., Bergstrom, H. K., McCloskey, B. D. & Mandadapu, K. K. Transport phenomena in electrolyte solutions: Nonequilibrium thermodynamics and statistical mechanics. *AIChE J.*

66, e17091 (2020).

5. He, X., Zhu, Y., Epstein, A. & Mo, Y. Statistical variances of diffusional properties from ab initio molecular dynamics simulations. *npj Comput. Mater.* **4**, 18 (2018).
6. Williams, S. R. & Evans, D. J. Linear Response Domain in Glassy Systems. *Phys. Rev. Lett.* **96**, 015701 (2006).
7. Nilsson, J. O. *et al.* Ionic conductivity in Gd-doped CeO_2: Ab initio color-diffusion nonequilibrium molecular dynamics study. *Phys. Rev. B* **93**, 024102 (2016).
8. Baktash, A., Reid, J. C., Roman, T. & Searles, D. J. Diffusion of lithium ions in Lithium-argyrodite solid-state electrolytes. *npj Comput. Mater.* **6**, 162 (2020).
9. Kobayashi, R., Nakano, K. & Nakayama, M. Non-equilibrium molecular dynamics study on atomistic origin of grain boundary resistivity in NASICON-type Li-ion conductor. *Acta Mater.* **226**, 117596 (2022).
10. Braga, C., Galindo, A. & Müller, E. A. Nonequilibrium molecular dynamics simulation of diffusion at the liquid-liquid interface. *J. Chem. Phys.* **141**, 154101 (2014).
11. Rahman, A. Correlations in the Motion of Atoms in Liquid Argon. *Phys. Rev.* **136**, A405 (1964).